Comparing free surface and interface motion in electromagnetically driven thin-layer flows

Benjamin C. Martell, Jeffrey Tithof, and Douglas H. Kelley*
Department of Mechanical Engineering, University of Rochester, Rochester, New York 14627, USA

(Received 21 July 2018; published 22 April 2019)

Two-dimensional fluid dynamics is often approximated via laboratory experiments that drive a thin layer of fluid electromagnetically. That approximation would be most accurate if both the direction and magnitude of the flow were uniform over the depth of the layer. In practice, boundary conditions require the flow magnitude to drop to zero at the no-slip floor, but put no strong constraint on flow direction. We measure the velocity magnitude and direction simultaneously at the free surface and lower interface of a thin, two-layer vortex flow. We find that the flow direction is almost entirely independent of depth, though its slight misalignment grows as the Reynolds number (Re) increases. Similarly, we find that the ratio of speeds at the free surface and interface nearly matches an analytically derived profile based on idealized assumptions, even for complex flows, but deviates systematically as Re increases. We find that flows with thinner fluid layers are better aligned and more nearly match the predicted speed ratio than flows with thicker layers. Finally, we observe that in time-dependent flows, flow structures at the interface tend to follow flow structures at the free surface via complicated dynamics, moving along similar paths with a short time delay. Our results suggest that the depth-averaged equation of motion recently developed for thin-layer flows [Suri *et al.*, Phys. Fluids **26**, 053601 (2014)], which relies on flow alignment and idealized profiles and was previously tested for Kolmogorov flows with Re up to 30, is reasonably accurate for vortex flows with Re up to 470.

DOI: 10.1103/PhysRevFluids.4.043904

I. INTRODUCTION

There are many good reasons to study two-dimensional (2D) fluid dynamics in a three-dimensional (3D) world. Many geophysical flows, occurring in contexts like oceans and atmospheres, are dominated by 2D motions because the horizontal extent of the fluid layer is far greater than its vertical depth, and because rotation and gravitational stratification further constrain vertical flow [1]. A rich theory of 2D turbulence predicts that at high Reynolds numbers (Re), 2D flows exhibit strikingly different physics than 3D flows. In the inviscid case, 2D flow conserves not only energy but also enstrophy (squared vorticity), giving rise to simultaneous turbulent cascades of energy to large length scales and enstrophy to small length scales [2–4]. Furthermore, 2D or quasi-2D flows provide useful models for exploring new physical insights from ideas like Lagrangian coherent structures (LCSs) [5–7], exact coherent structures (ECSs) [8,9], transfer of energy and enstrophy among length scales [10–13], and advection-reaction-diffusion mechanisms [14–19], because 2D simulations demand far less computational power than 3D simulations and making high-resolution measurements throughout an experimental domain is far easier in 2D than in 3D. Analysis is also less computationally demanding in 2D than in 3D, whether the data of

*d.h.kelley@rochester.edu

interest came from simulation or laboratory experiment. The review by Clercx and van Heijst [20] provides more detail.

Often, quasi-2D flow is produced in the laboratory by driving a thin layer of fluid electromagnetically. As was first shown many years ago [21], passing electrical current through a conductive fluid near an array of permanent magnets produces quasi-2D flow in an apparatus that is easy to build because it has no moving parts. The characteristic flow speed can be controlled by adjusting the current, and the spatial structure of the flow can be controlled by changing the magnet array. Common configurations include Kolmogorov flow, in which magnets are arranged with polarity alternating in stripes [22]; square lattices, in which polarity alternates like a checkerboard [23]; and quasirandom arrangements [24]. In all configurations, weak electrical currents drive low-Re flow that is steady and takes its shape from the magnet arrangement, but strong currents drive aperiodic flow that is more complicated both temporally and spatially.

However, studying 2D flow using 3D experimental devices is always an approximation whose fidelity must be considered and quantified. Devices are usually designed to minimize out-of-plane flow: fluid layers are chosen to have horizontal extent far greater than their depth, magnets and currents are arranged to minimize vertical electromagnetic forces, and tracer particles are often constrained by buoyancy to either the free surface of the fluid or an interface between two different fluid layers, stratified by gravity. But mechanisms like Ekman pumping [25] and shear instabilities [26] drive out-of-plane flow nonetheless. The magnitude of out-of-plane flow has been measured directly [27,28] and has been measured indirectly via decay times [29], via the normalized in-plane divergence [30], and by projecting measurements onto stream function modes [26]. One study found vertical flow variation that nearly matched Poiseuille flow, suggesting that out-of-plane motion is weak [31], but others found a poor match to Poiseuille flow, suggesting strong out-of-plane motion [27,28,30]. One study pointed out that centrifugal pressure variation causes layer thickness to vary across vortices, though the variation is typically negligible [32]. Another study showed that an apparent shear instability strengthens out-of-plane motion rapidly when Re exceeds a critical value near 200 [26]. We recently compared out-of-plane motion in three common configurations: a single thin layer, a miscible two-layer configuration in which the conductive fluid lies below a freshwater layer, and an immiscible two-layer configuration in which the conductive fluid lies above an oil layer. An apparent shear instability, similar to that reported in Ref. [26], was again found for the miscible two-layer configuration. No shear instabilities were apparent in the single-layer or immiscible configurations over a wide range of Re [33]. In another recent study, Suri *et al.* [34] derived an expression for the vertical profile of a quasi-2D Kolmogorov flow, based on idealized assumptions, and showed that it closely matched experimental measurements in steady flows with $\mathrm{Re} \leqslant 30$.

Here, we quantify 3D effects in quasi-2D flows by measuring horizontal velocity fields simultaneously at two different depths in the thin layer of fluid. In a truly 2D flow, no quantity would vary with depth, so the two velocity fields would match exactly. In typical laboratory experiments, they do not match exactly, because the floor underneath the fluid imposes a no-slip boundary condition, causing the speed to be zero there. Speed varies with depth. However, the horizontal flow direction is not constrained by the boundary condition at the floor, and one might imagine the horizontal flow direction being independent of depth (though secondary flows like Ekman pumping do affect direction and are indirect consequences of boundaries). In this paper, we compare horizontal speed and direction at the free surface of a thin layer to speed and direction at the interface between that layer and a lubrication layer below. We experiment with both steady and time-dependent flows, driven using a square lattice of magnets. We find that the directions of the two velocity fields are closely aligned nearly everywhere, but alignment decreases as Re increases. We find that the ratio of the speed at the interface to that at the free surface varies over space and time, with its most likely value falling within about 16% of the value for an analytically-derived velocity profile based on idealized assumptions [34], matching closest where the flow directions are aligned. As Re increases, the speed at the free surface increases faster than the speed at the interface, i.e., the speed ratio decreases. Thinner layers provide better alignment and speed ratios that match the idealized

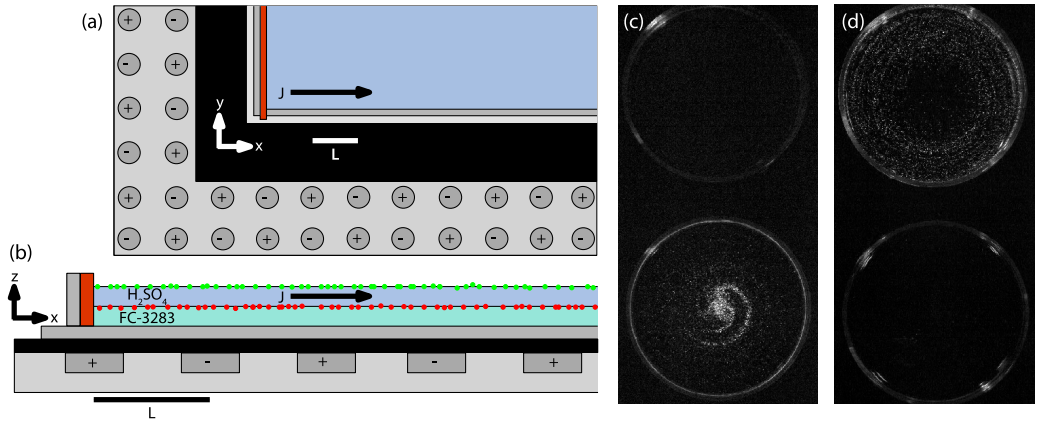

FIG. 1. The experimental apparatus and its imaging capability. (a) A view from above shows the magnet grid, glass sheet, and experimental vessel, with one electrode visible at left. Magnet polarity is indicated by + or −. The direction of the current density $\boldsymbol{J}$ is indicated with a black arrow. (b) A cross-section shows green and red tracer particles at the free surface and oil-acid interface, respectively. (c) The view through a filter blocking red shows only green particles, which are in the dish at bottom in the image. (d) The view through a filter blocking green shows only red particles, which are in the dish at top in the image.

profile more closely. Finally, we observe that flow features at the interface often follow flow features at the free surface, via complicated temporal dynamics.

Below, the paper continues with a description of our experimental methods in Sec. II. Our results are presented in Sec. III. A summary, a discussion of the implications of our results, and a few ideas for future work are given in Sec. IV.

II. EXPERIMENTAL METHODS

Our methods are similar to those described previously [33], and our experimental device is sketched in Figs. 1(a) and 1(b). We drive flow in a thin, conductive layer of 1 M sulfuric acid (density $\rho = 1.06\,\mathrm{g/cm^3}$ and viscosity $\mu = 1.19 \times 10^{-3}$ Pa s) floating atop a layer of FC-3283 oil (density $\rho = 1.75\,\mathrm{g/cm^3}$ and viscosity $\mu = 1.42 \times 10^{-3}$ Pa s), which acts as a lubrication layer. The two layers are immiscible, and we use acid instead of salt water because its higher conductivity reduces thermal effects due to Joule heating. Both layers are contained by a square tray with lateral dimensions 254×254 mm. To induce motion, we pass an electrical current, with density ranging from 33 to $1200\,\mathrm{A/m^2}$, in the $\hat{\boldsymbol{x}}$ direction through the acid layer between two identical copper electrodes spanning opposite sides of the tray. That current produces local forces by interacting with the magnetic fields of a square array of cylindrical NdFeB magnets below the floor of the tray, arranged in a checkerboard pattern. Each magnet has diameter 12.7 mm, has thickness 3 mm, lies with its center $L = 25.4$ mm from those of its four nearest neighbors, and has magnetic field 0.3 T near its face. The acid and oil layers have identical thickness $h/2 = 6$ mm in some experiments and $h/2 = 3$ mm in others, as specified below.

Our methods differ from previous studies in that we simultaneously measure flow at the free surface and interface. To do so, we seed the top surface with green tracer particles (Cospheric UVPMS-BG-1.025, diameter 90 to 106 μm, density $1.022\,\mathrm{g/cm^3}$) and seed the bottom surface with red tracer particles (Cospheric UVPMS-BR-1.20, diameter 75 to 90 μm, density $1.211\,\mathrm{g/cm^3}$). Gravity keeps the particles at their respective surfaces because the green particles are less dense than the acid, whereas the red particles have density intermediate between that of the acid and the oil. The particles are small enough to track fluid motion faithfully. Surface tension at both the free surface and the interface tends to cause particles to aggregate, with the primary effect that

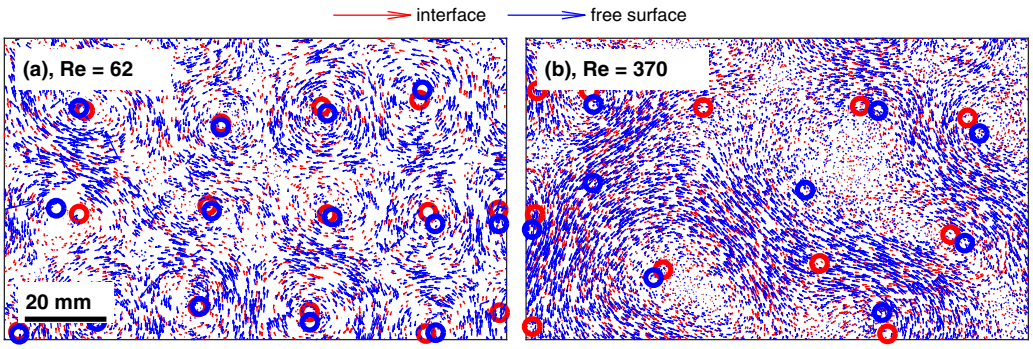

FIG. 2. Instantaneous velocity measurements at the free surface and interface. Each arrow indicates the position and velocity of one tracked particle; color indicates whether the particle followed fluid motion at the free surface or at the interface. Circles indicate vortex centroids at the top and bottom of the acid layer, located using an algorithm described below. Both snapshots show the same region, which covers 17% of the area visible to both cameras. The snapshots come from experiments using 6-mm layers at (a) $\mathrm{Re} = 62$ and (b) $\mathrm{Re} = 370$. By simultaneously tracking particles at the free surface and interface, we can quantify the variation of velocity with depth, even in time-dependent flows.

our measurement count is reduced, and the secondary effect that tracers track the flow slightly less faithfully because they are effectively larger. We reduce aggregation by adding a few drops of surfactant. We record the motion of each set of particles using a dedicated camera. One camera images only green particles because it is equipped with a color filter that blocks red [Fig. 1(c)]; the other camera images only red particles because its filter blocks green [Fig. 1(d)]. The cameras (Emergent HS-4000M) produce images with size 2048×2048 pixels and are synchronized in hardware. We vary the frame rate from 60 to 90 Hz as necessary to avoid blurring. The two cameras hang side-by-side, so their fields of view differ. We image a calibration target with both cameras, then use a least-squares algorithm to determine the translation and (small) rotation that best align the two images. We use that translation and rotation, along with the known size of the calibration target, to express all experimental measurements in a common coordinate system using metric units, discarding measurements outside the region visible to both cameras. Our alignment procedure is the same as the one used previously to align one set of particle tracking measurements with images of solution color in advection-reaction-diffusion experiments [15].

We track particles in the resulting movies using an established algorithm [35], producing velocity measurements like those shown in Fig. 2. In Sec. III, we will compare these simultaneous measurements at the free surface and interface to predictions obtained by numerically computing the idealized vertical profiles of the in-plane velocity following the procedure of Suri *et al.* [34]. These profiles, shown in Fig. 3, closely resemble profiles of Poiseuille flow and are derived with the assumption that the in-plane velocity: (i) has direction that is perfectly uniform along the layer depth and (ii) varies sinusoidally along one direction (i.e., the flow corresponds to steady Kolmogorov flow). Despite these restrictive assumptions and the fact that we focus on aperiodic checkerboard flow, the results below will demonstrate reasonable agreement with these velocity profiles.

The Reynolds number of each experiment is defined as $\mathrm{Re} = UL/\bar{\nu}$, where U is the measured root-mean-square velocity of tracked particles at the free surface and $\bar{\nu}$ is the depth-averaged viscosity introduced by Suri *et al.* [34]. By computing $\bar{\nu}$, we define the Reynolds number in such a way that accounts for the different kinematic viscosities of the two fluid layers. Particle tracking produces velocity measurements at particle locations, which are typically irregular, as Fig. 2 shows. To compare the flow at the free surface to the flow at the interface, we interpolate both sets of measurements onto the same regular grid, with grid spacing 3 mm, using a linear interpolation

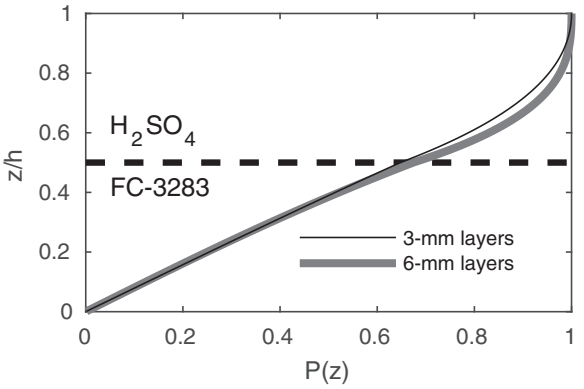

FIG. 3. Idealized velocity profiles computed using the method of Suri *et al.* [34] with depths matching our experiments. Profiles for different layer thicknesses differ slightly, primarily because the magnetic field decays along z. The ratio of interface speed to free-surface speed is $s^{-1} = 0.675$ for 6-mm layers and 0.648 for 3-mm layers.

scheme. We also test for outliers using a standard algorithm [36] and replace them via linear interpolation.

III. RESULTS

As Fig. 2 and Supplemental Material movies S1 and S2 show [37], the flows at the top and bottom of the conductive fluid are similar, but not identical, and differ more as Re increases. Since boundary conditions do not explicitly affect the *direction* of horizontal flow, one might expect it to be independent of depth, and we begin by testing that hypothesis. The angle θ between the flow directions at the free surface and interface of the fluids quantifies alignment:

$$\cos\theta = \frac{\boldsymbol{V}(x, y, h/2, t) \cdot \boldsymbol{V}(x, y, h, t)}{|\boldsymbol{V}(x, y, h/2, t)|\,|\boldsymbol{V}(x, y, h, t)|}. \tag{1}$$

Here $\boldsymbol{V}(x, y, z, t)$ is the horizontal velocity, varying with Cartesian spatial coordinates (x, y, z) and time t. The vertical coordinate z is zero at the floor of the fluid container and increases upward. Two typical snapshots of the alignment $\cos\theta$ are shown in Fig. 4; they are taken from the same experiments, same times, and same regions as the velocity measurements shown in Fig. 2. The flows at the free surface and interface are nearly aligned ($\cos\theta \approx 1$) almost everywhere. Antialignment ($\cos\theta \approx -1$) occurs almost exclusively near stagnation points, where the velocity is zero. Mathematically, at those isolated points, $\cos\theta$ is undefined because the velocity direction is undefined. In practice, in regions near those isolated points, $\cos\theta$ is noisy because the velocity magnitude is small, reducing the accuracy of any measurements. Thus, apparent antialignment near stagnation points tells little about flow dynamics and deserves little attention. That said, the free surface and interfacial flows clearly align better at lower Re.

Our observations from snapshots of alignment are consistent with the statistics of $\cos\theta$, shown in Fig. 5. We calculated the alignment $\cos\theta$ in a 120×138 mm region in 19 different experiments, all with 6-mm layers, lasting between 45 s and 63 s, at Reynolds numbers varying from $\mathrm{Re} = 62$ to $\mathrm{Re} = 470$. For every experiment, the statistical distribution peaks at $\cos\theta = 1$, showing that close alignment is most likely. Misalignment is less likely at low Reynolds numbers than at high Reynolds numbers. That fact is consistent with intuition: as Re increases, flows fluctuate more rapidly in time and space, and therefore deviate further from the steady flows for which the alignment assumption seems most reasonable. Moreover, fast fluctuations leave too little time for viscous coupling to bring the motion of the oil layer into alignment with the motion of the driven layer. A minor peak in the

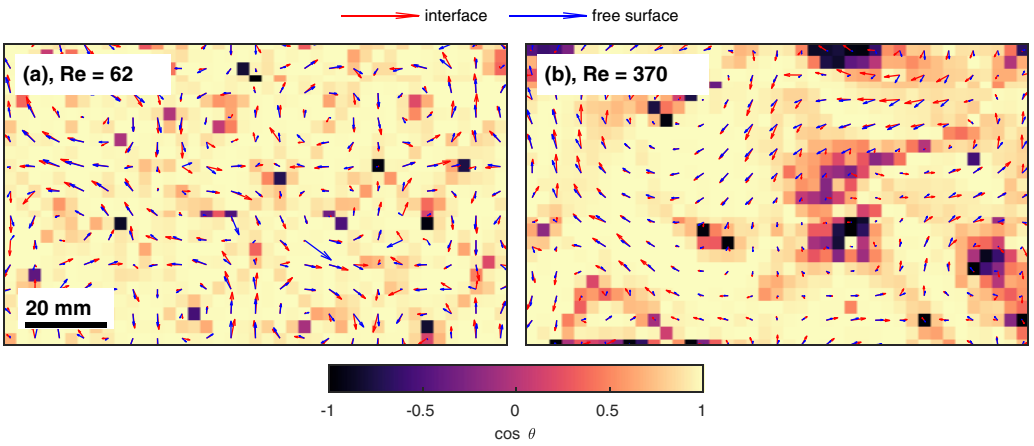

FIG. 4. Instantaneous alignment $\cos\theta$ at (a) $\mathrm{Re} = 62$ and (b) $\mathrm{Re} = 370$, in the same region and at the same times shown in Fig. 2, from the same experiments with 6-mm layers. Arrows indicate velocity fields at the interface and free surface. Anti-alignment ($\cos\theta \approx -1$) occurs only near singularities where the surface speed is almost zero.

distributions, still more than an order of magnitude lower than the main peak, occurs at $\cos\theta = -1$; we attribute it to the fact, discussed above, that accurate measurement is impossible near stagnation points. Hence, we have plotted median values rather than mean values of the alignment, which are less skewed by these outliers. The median alignment is 0.92 or greater for all experiments and is highest at low Reynolds numbers.

Having shown that the flow direction is not strictly independent of depth, but the two flows are closely aligned at most places over a range of Reynolds numbers, we now consider the flow speed, and particularly the ratio of the speed at the interface to the speed at the free surface,

$$s^{-1} = \frac{|\boldsymbol{V}(x, y, h/2, t)|}{|\boldsymbol{V}(x, y, h, t)|}. \tag{2}$$

The variation of speed with depth depends on the forcing (magnet arrangement) and fluid properties, but for a typical two-layer immiscible configuration we expect it to vary monotonically from zero at

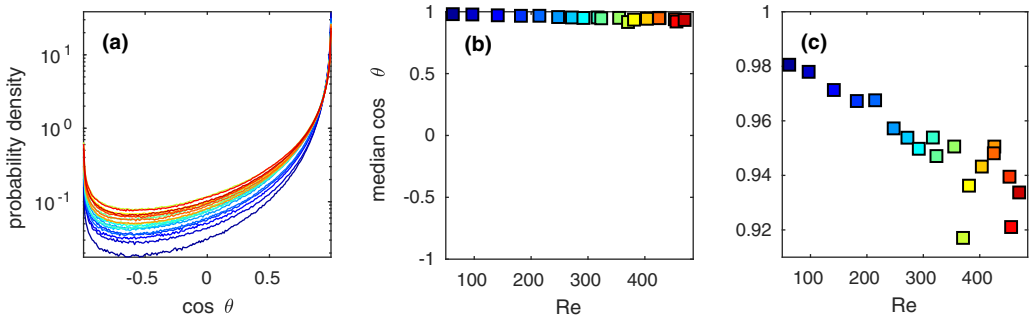

FIG. 5. Statistics of alignment $\cos\theta$, in experiments with 6-mm layers. (a) Distributions of $\cos\theta$ from 19 experiments at different Reynolds numbers, plotted on a logarithmic scale, show that near-alignment ($\cos\theta \approx 1$) is most common. (b) The median value of $\cos\theta$ is near 1 in all 19 experiments. (c) An enlargement of the same data shown in (b) demonstrates systematic variation with Re. Colors in (a) correspond to symbol colors in (b), (c) and indicate Re.

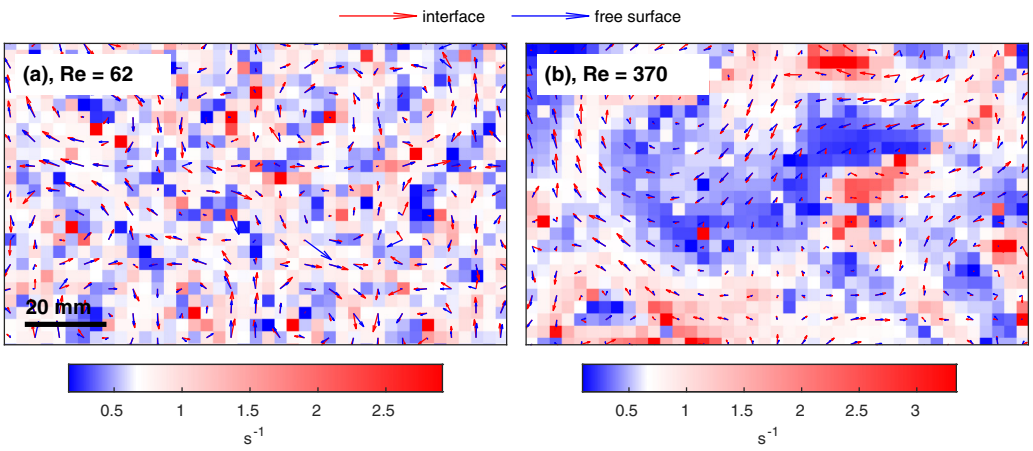

FIG. 6. Instantaneous speed ratio s^{-1} at (a) Re = 62 and (b) Re = 370, in the same region and at the same times shown in Fig. 2, from the same experiments with 6-mm layers. Blue regions have speed ratio lower than the theoretical prediction; red regions, higher. Arrows indicate velocity fields at the interface and free surface. The speed ratio is large near singularities where the surface speed is almost zero, but nearly matches the value for an idealized profile in most places.

the no-slip bottom of the fluid layers to some maximum speed at the free surface. Thus s^{-1} can be interpreted as the interface speed (at $z = h/2$), normalized by the free-surface speed (at $z = h$), and typically $s^{-1} \leqslant 1$. In the case of an idealized velocity profile (Fig. 3), s^{-1} has a value that can be calculated exactly. For our configuration with 6-mm layers, an idealized profile would have speed ratio $s^{-1} = 0.675$; for 3-mm layers, $s^{-1} = 0.648$. Normalizing by the speed at the free surface is also convenient because we define the Reynolds number based on motion there. We name the ratio s^{-1} such that our notation is consistent with that of Suri *et al.*, who dealt with its inverse, s.

Two typical snapshots are shown in Fig. 6; they are taken again from the same experiments, same times, and same regions as the velocity measurements in Fig. 2. Over much of the flow, theory accurately predicts the measured speed ratio. It is significantly larger than the theoretical prediction in small regions that usually correlate with poor alignment (compare to Fig. 4). The speed ratio is lower than predicted only in small regions of the Re = 62 snapshot, but in much larger regions of the Re = 370 snapshot. That is, the higher-Re flow is measurably less two-dimensional, since a perfectly 2D flow would have $s^{-1} = 1$.

The statistics of s^{-1}, shown in Fig. 7, support our observations from snapshots. We calculated s^{-1} in the same region in the same 19 experiments with 6-mm layers, over the same durations. In Fig. 7(a), we have plotted distributions of s^{-1} for a range of Re, which shows that s^{-1} varies from values much smaller than the value predicted by an idealized velocity profile, to much larger values. However, the distributions of s^{-1} calculated from low-Re experiments peak almost exactly at the value for an idealized velocity profile. As Re increases, the most likely values (peak locations), plotted in Fig. 7(b), move to lower values of s^{-1} systematically, confirming that higher-Reynolds-number flows are less 2D. The median values of s^{-1} follow the same trend as the most likely values. We have plotted the median and most likely values here, but not the mean value, which can be substantially skewed by the few very large s^{-1} outliers arising where the free surface speed is nearly zero.

We have shown that the velocity fields at the free surface and interface are often nearly aligned but do deviate from $\cos\theta = 1$, and that the speed ratio s^{-1} often falls close to the value predicted [34] for a steady, idealized flow, but does deviate from that value. It is natural to ask whether the two observations are related. In particular, since $\cos\theta = 1$ is an assumption necessary for deriving the idealized vertical flow profile, we might wonder if the speed ratio deviates most from its

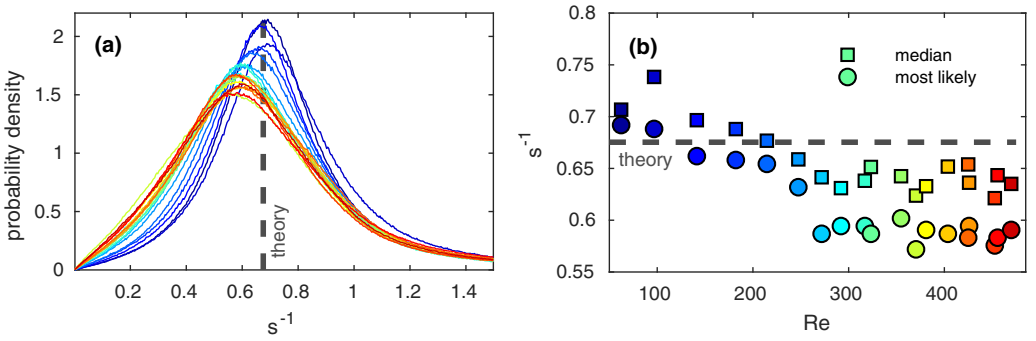

FIG. 7. Statistics of speed ratio s^{-1} in experiments with 6-mm layers. (a) Distributions of s^{-1} from the same 19 experiments characterized in Fig. 5. (b) Median and most likely values of s^{-1}, varying with Re. Colors in (a) correspond to symbol colors in (b) and indicate Re. In all cases, the most likely value of s^{-1} falls within 11% of the value $s^{-1} = 0.675$ expected for an idealized profile with 6-mm layers. However, typical values of s^{-1} drop systematically as Re increases, showing that the steady case becomes a poorer approximation as flows become more turbulent.

predicted value when alignment is poor. Figure 8 shows that it does. The figure displays the mean and median values of s^{-1}, conditioned on $\cos\theta$. That is, in each of the same 19 experiments, we located all the times and places where $\cos\theta$ fell near a particular value, and calculated the mean and median values of s^{-1} for those times and places. We repeated the calculations over the whole range of values $-1 \leqslant \cos\theta \leqslant 1$. Remarkably, for experiments at any Reynolds number, the mean and median values of the speed ratio s^{-1} nearly match the theoretical prediction when the alignment $\cos\theta \approx 1$. As $\cos\theta$ decreases, median values of s^{-1} stay within a few percent of the prediction, but mean values of s^{-1} grow significantly, roughly doubling the prediction where $\cos\theta = -1$. A distribution whose median changes little but whose mean changes significantly is becoming more skewed; as the alignment becomes poorer, the speed ratio remains close to the prediction in most places, but becomes increasingly large in a few places. Figure 8 also shows that increasing Re reduces s^{-1}, consistent with the snapshots of Fig. 6 and the distributions of Fig. 7. Interestingly,

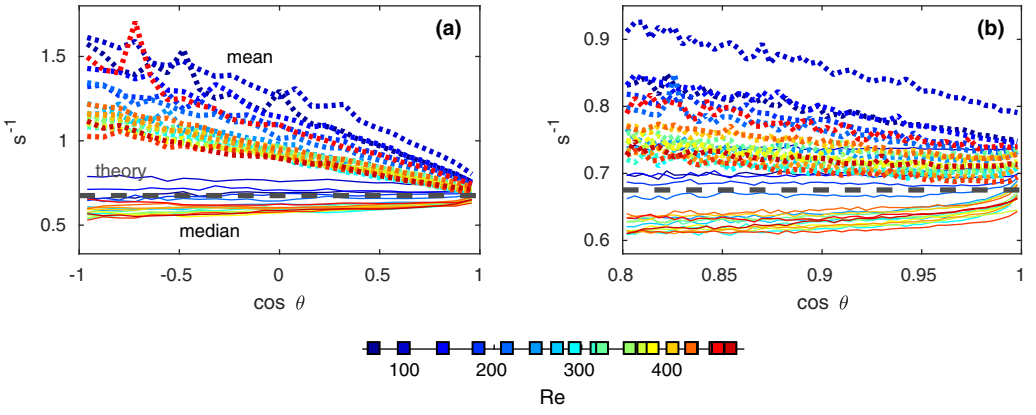

FIG. 8. Statistics of speed ratio s^{-1}, conditioned on $\cos\theta$, in experiments with 6-mm layers. Median values appear as thin lines, mean values appear as dotted lines, and the value for an idealized profile appears as a dashed line. Colors indicate varying Reynolds numbers, as in Fig. 5. Panel (a) shows the entire range $-1 \leqslant \cos\theta \leqslant 1$; panel (b) shows the range $0.8 \leqslant \cos\theta \leqslant 1$. The speed ratio s^{-1} decreases as Re increases. When $\cos\theta \approx 1$, mean and median values of s^{-1} nearly match the value for an idealized profile.

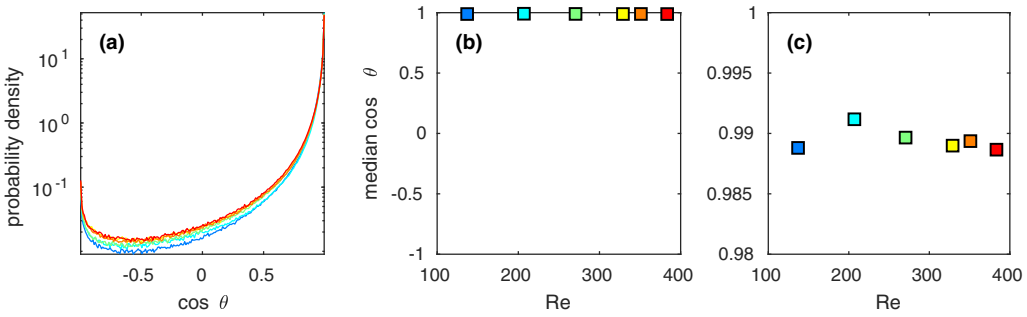

FIG. 9. Statistics of alignment $\cos\theta$, in experiments with 3-mm layers. (a) Distributions of $\cos\theta$ from six experiments at different Reynolds numbers, plotted on a logarithmic scale, show that near-alignment ($\cos\theta \approx 1$) is most common. (b) The median value of $\cos\theta$ is near 1 in all experiments. (c) An enlargement of the same data shown in (b) demonstrates systematic variation with Re. Colors in (a) correspond to symbol colors in (b, c) and indicate Re.

since increasing Re and decreasing $\cos\theta$ have opposite effects on the mean value of s^{-1}, the speed ratio of misaligned regions falls closer to the theoretical prediction at high Reynolds number than at low Reynolds number.

One of the mechanisms that reduces out-of-plane motion in quasi-2D experiments is the aspect ratio of the fluid layer; flows in thinner layers tend to involve weaker out-of-plane motion [20]. We therefore wondered if, in thinner layers, the flows at the interface and free surface would be better aligned, and their speed ratio s^{-1} would more closely match the value for an idealized profile. To address that question, we performed experiments similar to the ones described above, but with $h/2 = 3$ mm, instead of 6 mm. We again calculated the alignment $\cos\theta$ in a 120×138 mm region, now with 3-mm layers, in six experiments lasting 30 s each, at Reynolds numbers varying from $\mathrm{Re} = 137$ to 383. The resulting statistics are shown in Fig. 9. Distributions of $\cos\theta$ are similar to the 6-mm case, but the minor peaks at $\cos\theta = -1$ are weaker, and the minima near $\cos\theta = -0.6$ are lower. Accordingly, the median values of $\cos\theta$ are closer to unity (compare to Fig. 5).

We also calculated statistics of the speed ratio s^{-1} in the experiments with 3-mm layers, as shown in Fig. 10. For these thinner layers, distributions of s^{-1} peak near the theoretical prediction for the entire range of Re explored. Median values of s^{-1} stay closer to the theoretical prediction than in experiments with 6-mm layers (compare to Fig. 7). Thus, these experiments are more nearly 2D, in

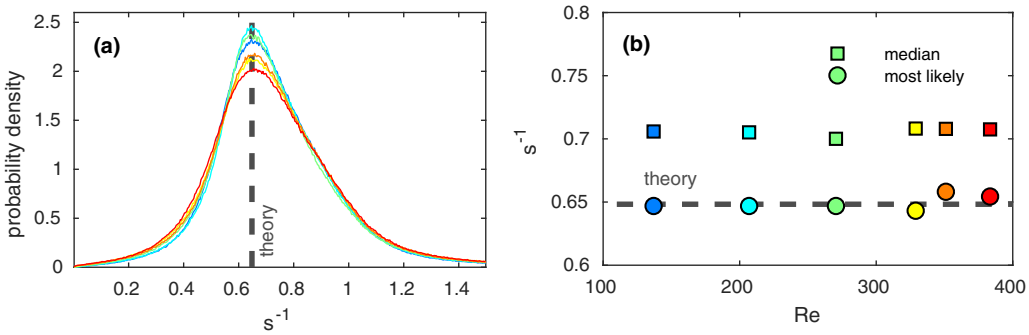

FIG. 10. Statistics of speed ratio s^{-1} in experiments with 3-mm layers. (a) Distributions of s^{-1} from the same six experiments characterized in Fig. 9. (b) Median and most likely values of s^{-1}, varying with Re. Colors in (a) correspond to symbol colors in (b) and indicate Re. In all cases, the mostly likely value of s^{-1} falls within 2% of the value $s = 0.648$ expected for an idealized profile with 3-mm layers.

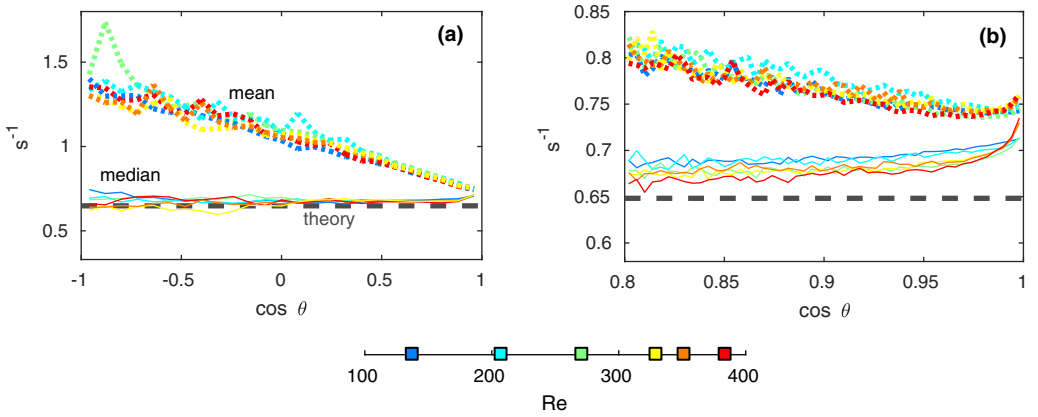

FIG. 11. Statistics of speed ratio s^{-1}, conditioned on $\cos\theta$, in experiments with 3-mm layers. Median values appear as thin lines, mean values appear as dotted lines, and the value for an idealized profile appears as a dashed line. Colors indicate varying Reynolds numbers, as in Fig. 9. Panel (a) shows the entire range $-1 \leqslant \cos\theta \leqslant 1$; panel (b) shows the range $0.8 \leqslant \cos\theta \leqslant 1$. The speed ratio s^{-1} decreases as Re increases.

the sense that the flows at the interface and free surface are better aligned and the speed ratio more nearly matches an idealized profile, when the fluid layer is thinner.

Figure 11 shows statistics of s^{-1} conditioned on $\cos\theta$ in experiments with 3-mm layers. The trends are similar to those observed in experiments with 6-mm layers (compare to Fig. 8): s^{-1} matches the idealized value most closely when $\cos\theta \approx 1$; as $\cos\theta$ decreases, the median value of s^{-1} changes little, but the mean value increases significantly; and s^{-1} drops as Re increases. However, the effect of Re is weaker in experiments with 3-mm layers, as shown by the fact that the curves are clustered more tightly in Fig. 11 than in Fig. 8.

Though our measurements show that the speed ratio s^{-1} does deviate from the value for an idealized velocity profile, that profile is often a good approximation, consistent with prior results [34]. This result is somewhat surprising: the idealized profile (Fig. 3) is strictly applicable only for a velocity field in which the flow direction is perfectly aligned along the depth of the fluid and the in-plane velocity profile corresponds to laminar Kolmogorov flow. This is in contrast with the time-dependent, square lattice of vortices we study here. Nonetheless, to examine the accuracy of the predictions made by this idealized profile, we quantify the relative error ϵ:

$$\epsilon = \frac{s^{-1}_{\text{measured}} - s^{-1}_{\text{idealized}}}{s^{-1}_{\text{idealized}}}. \tag{3}$$

Figure 12 plots ϵ as it varies with Re, for experiments with both 6- and 3-mm layers, allowing quantitative comparison. Median values are higher than most-likely values, consistent with the skew in s^{-1} discussed above. As expected, the speed ratio more nearly matches the theoretical prediction in experiments with 3-mm layers than in experiments with 6-mm layers. The ratio also varies less in 3-mm layers, consistent with the consensus that thinner layers are better approximations to 2D flow [20]. Based on the most likely value of s^{-1}, we find $\epsilon \leqslant 16\%$ for the 6-mm layers, while the 3-mm layers provide a substantial improvement with $\epsilon \leqslant 2\%$.

We have used the alignment $\cos\theta$ and the speed ratio s^{-1} to quantify the *instantaneous* relationship between motion at the top and bottom of the conductive layer in our experiments. The time dynamics linking motions at the top and bottom are also interesting. Electromagnetic forces drive the acid layer, which is coupled to the oil layer via viscosity. For steady, fully-developed flows, we would expect the velocity of the oil layer to have a spatial structure closely matching the acid layer [though with a lower speed, consistent with Fig. 3 and Eq. (2)]. For flows varying slowly in

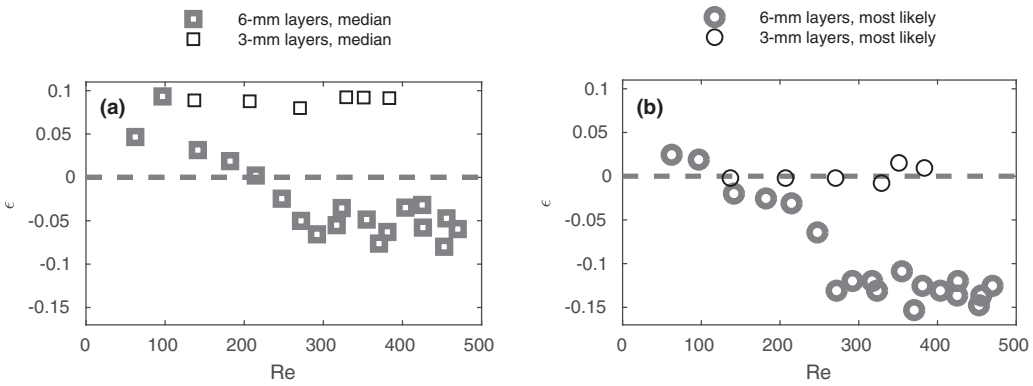

FIG. 12. Comparison of the speed ratio relative error ϵ for different layer thicknesses. (a) Speed ratio relative error for median s^{-1} varying with Re for both 6-mm and 3-mm layers. (b) Speed ratio relative error for most likely s^{-1} varying with Re for both 6-mm and 3-mm layers. For thinner layers, the error in the most likely value of s^{-1} is lower, although the error in the median value is higher.

time, the match between oil and acid would be nearly as good. As flows vary more rapidly, however, we would expect a poorer match, because viscous forces are allowed shorter times in which to affect the oil layer before the flow changes. That expectation is confirmed by many of the results described above, which show that increasing Re tends to reduce $\cos\theta$ and s^{-1}. However, considering viscous coupling as the mechanism, we can go further: for time-dependent flows, we would expect motion at the acid-oil interface to lag behind motion at the free surface of the acid layer.

Careful examination of the evolution of velocity fields at the free surface and interface of the configuration with 6-mm layers in the same experiment with $\mathrm{Re} = 370$ (Supplemental Material movie S2 [37]) shows that motion at the interface does often lag behind motion at the free surface. The two velocity fields have similar structures, with regions of rotation and strain often taking similar shapes and occurring at similar places. Those regions sometimes move in complicated ways that often appear to involve the interface lagging behind the free surface. In the experiment with $\mathrm{Re} = 62$, which is almost steady, flow structures are again similar, but the interface seems to lag behind the free surface much less (Supplemental Material movie S1 [37]).

To quantify the time dynamics linking motions at the free surface and interface, we identified flow structures using the Okubo-Weiss criterion [38,39]:

$$Q(x, y) = \det \begin{bmatrix} \partial_x u_x & \partial_y u_x \\ \partial_x u_y & \partial_y u_y \end{bmatrix}. \tag{4}$$

When $Q > 0$, the vorticity exceeds the strain rate; when $Q < 0$, the strain rate exceeds the vorticity. Thus, regions where $Q \geqslant Q_0 > 0$, with Q_0 being a chosen threshold, reasonably approximate vortex cores. The Okubo-Weiss criterion is not an objective quantity, nor even Galilean-invariant [40]. Great progress in recent years has produced methods that can identify flow structures more rigorously and in frameworks that are properly Lagrangian [5,6]. Such methods could locate vortex cores with greater accuracy, at the expense of methodological complexity and computational effort. However, our interest is not in the detailed mixing dynamics of these flows, but only in labeling flow structures to compare their time dynamics, so we use Q for its simplicity and expediency.

Figure 13 shows snapshots of Q, taken from the same experiments, same times, and same regions as the velocity measurements in Fig. 2. Comparing the two figures shows that $Q > 0$ regions correlate with rotation. Choosing Q_0 as the 75th percentile of Q in each experiment, we defined each region Γ where $Q \geqslant Q_0$ as a vortex, unless its area was less than 25 mm^2. We calculated the

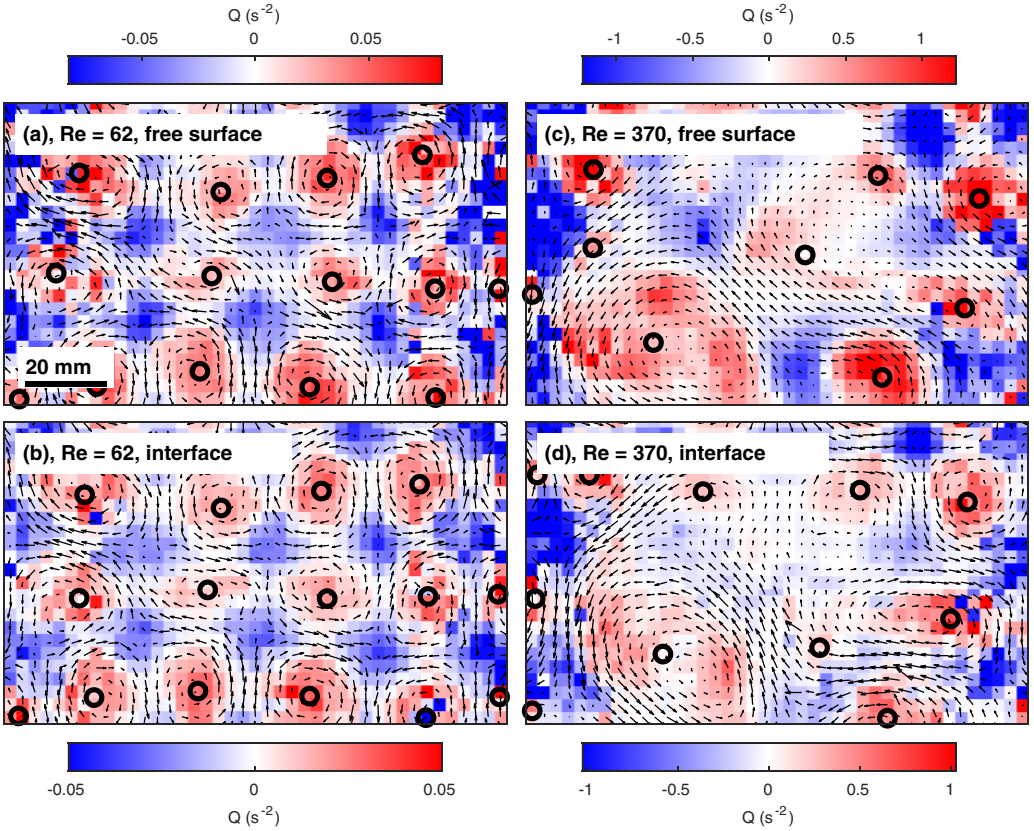

FIG. 13. Snapshots of the Okubo-Weiss criterion Q and vortex centroids. (a), (b) Snapshots at the free surface and interface, respectively, in the same experiment, at the same time, and in the same region as Fig. 2(a). (c), (d) Snapshot at the free surface and interface, respectively, in the same experiment, at the same time, and in the same region as Fig. 2(b). Corresponding velocity fields are indicated with arrows. $Q > 0$ in regions where rotation dominates shear, and the weighted centroids of regions identified as vortices are plotted as circles.

weighted centroid of each vortex, with location (x_c, y_c) given by

$$x_c = \frac{\int_\Gamma x\, Q(x,y)\, dA}{\int_\Gamma Q(x,y)\, dA}, \quad y_c = \frac{\int_\Gamma y\, Q(x,y)\, dA}{\int_\Gamma Q(x,y)\, dA}, \tag{5}$$

where $\int_\Gamma dA$ signifies an area integral over the region Γ. Those centroids are also plotted in Fig. 13.

By repeating those calculations for all velocity fields measured in the Re $= 370$ experiment with 6-mm layers, we located vortex centroids as they moved over time. We tracked them with the same particle tracking algorithm used for our velocity measurements, and a few of the resulting tracks are shown in Fig. 14. At this relatively high Reynolds number, vortices take complicated paths through the flow. Still, vortex centroids at the interface often trace similar paths to their nearest neighbors at the free surface. Moreover, vortex paths at the interface lag vortex paths at the free surface, suggesting that our expectations about viscous coupling are correct.

We also found the Okubo-Weiss parameter for all velocity fields measured in the other 18 experiments with 6-mm layers, at the free surface and at the interface, then compared the results to the local alignment. Specifically, we calculated the median value of $\cos\theta$, conditioned on Q/σ_Q (where σ_Q is the standard deviation of Q). As Fig. 15 shows, alignment is best at times and places where $Q \approx 0$—that is, where vorticity and strain are nearly balanced. Conversely, alignment is worst

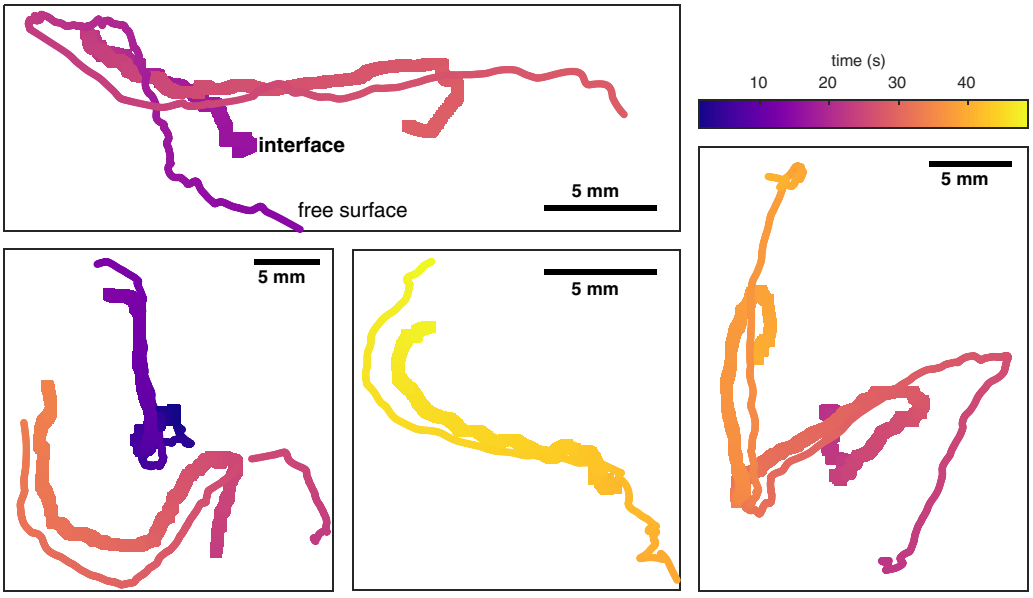

FIG. 14. Paths of coupled vortices at the free surface and interface, all from the Re = 370 experiment with 6-mm layers. Each curve shows the path of the weighted centroid of a region identified as a vortex, with thinner curves indicating vortices on the free surface and thicker curves indicating vortices at the interface. Time is indicated in color. In these and many other examples, vortices appear to be coupled, with a vortex at the interface moving along a similar path to a nearby vortex at the free surface, with some lag.

near stagnation points, where either vorticity dominates strain, or vice-versa. As Re increases, $\cos\theta$ drops, consistent with Fig. 5. At high Reynolds numbers, the curves become asymmetric: alignment is better where vorticity exceeds the strain rate at the free surface and better where strain rate exceeds vorticity at the interface.

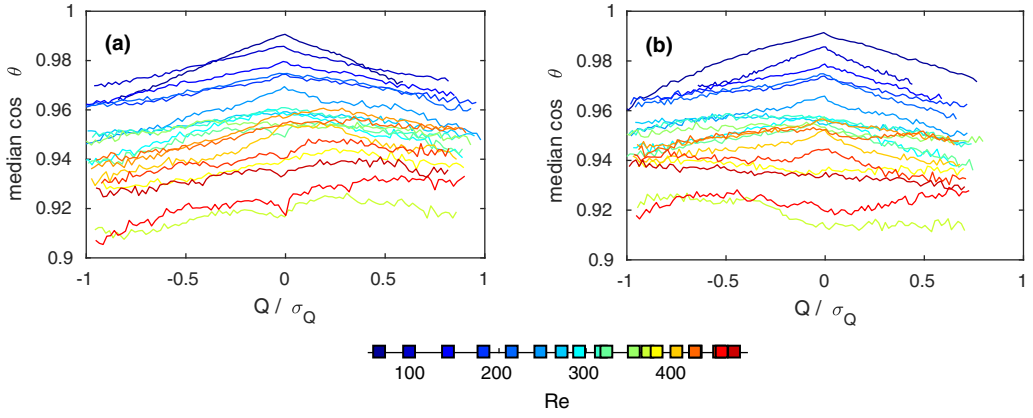

FIG. 15. Statistics of alignment $\cos\theta$, conditioned on Okubo-Weiss parameter Q normalized by its standard deviation σ_Q, at (a) the top of the acid layer, and (b) the bottom of the acid layer, in experiments with 6-mm layers. Colors indicate varying Reynolds numbers, as in Fig. 5. Alignment is best near $Q = 0$, where vorticity and strain are nearly balanced.

IV. SUMMARY AND CONCLUSIONS

We have compared motion at the free surface and the acid-oil interface in electromagnetically driven thin-layer flows to determine how well those flows can be modeled as 2D, focusing on the alignment and speed ratio. To measure the motions, we placed tracer particles of different colors at the two surfaces and tracked both simultaneously. Our experiments spanned a range of Reynolds numbers $62 \leqslant \mathrm{Re} \leqslant 470$ and used both thick ($h/2 = 6$ mm) and thin ($h/2 = 3$ mm) layers. In a strictly 2D system, the horizontal velocities at the two surfaces would have the same direction everywhere. We found that approximating the two flows to be aligned ($\cos\theta = 1$) is accurate within 6% for 6-mm layers and within 1% for 3-mm layers. Alignment is better at low Reynolds numbers; for example, a $\mathrm{Re} = 62$ experiment with 6-mm layers shows just 2% error. In a fluid experiment with a no-slip floor, the horizontal speeds at the two surfaces typically differ. We found that an idealized in-plane velocity profile along the vertical direction provides a good approximation for these unsteady, chaotic flows ($s^{-1} = 0.675$ for 6-mm layers and $s^{-1} = 0.648$ for 3-mm layers), which is accurate to within 16% for 6-mm layers and within 2% for 3-mm layers. Again, the match is better for 6-mm layers if the Reynolds number is lower. We also found that s^{-1} closely matches the idealized value in regions where $\cos\theta \approx 1$, regardless of the Reynolds number or layer thickness. Movies of our experiments suggest that flow features at the interface resemble and follow features at the free surface. We used the Okubo-Weiss parameter Q to locate flow features, and by tracking vortex centroids, showed that interface vortices do follow free-surface vortices along complicated paths and for long durations. Finally, we showed that alignment is best where strain rate and vorticity are nearly balanced ($Q \approx 0$), at both the free surface and the interface.

To our knowledge, these are the first simultaneous measurements of flow at both the free surface and the interface of thin-layer flows. We used these measurements to compare free-surface and interface velocities in terms of their alignment and speed ratio. Suri *et al.* [34] made idealized assumptions that the in-plane velocity was perfectly aligned throughout the depth of the fluid and that the in-plane velocity profile matched Kolmogorov flow (i.e., was sinusoidal along one direction), which allowed the authors to express the 3D velocity as the product of an in-plane 2D velocity times a vertical profile. Those authors went on to measure the speed ratio s in steady, Kolmogorov flows with $\mathrm{Re} \leqslant 30$, finding good agreement with the value for the idealized profiles [34]. We found near matches in steady and unsteady checkerboard flows (square lattices of vortices) over a wider range of Re. We emphasize that the near match persisted despite significant differences in the form of the in-plane forcing, time dependence, and Reynolds numbers of the flows. Good alignment between the free-surface and interface velocity fields also persisted throughout our experiments. Idealized profiles and alignment were assumed by Suri *et al.* to develop depth-averaged equations of motion. Recent studies [9,41] showed that simulations of the depth-averaged equations match experiments strikingly closely for $\mathrm{Re} \leqslant 22.5$. Our results strongly suggest that close matches are achievable at much higher Reynolds numbers, opening the way for exploring new physics with the benefit of tight coupling between simulation and experiment.

In future work, simultaneous velocity field measurements at the free surface and interface may prove useful for quantifying the accuracy of simulations based on the depth-averaged equations. Such measurements may also prove useful in making further improvements to 2D modeling, as they could be used to parametrize or validate theoretical estimates of effective depth-averaged parameters, which could be systematically varied with Re to achieve better agreement between experiment and 2D simulation. It may also prove useful to compute effective depth-averaged parameters that vary in space and time based on the local structure of the velocity field. In particular, Q might serve as a guide for such variation. We find that the alignment of the velocity at the free surface and interface is best ($\cos\theta \approx 1$) where $Q \approx 0$, which suggests that the current modeling is most accurate where rotation and strain are approximately balanced. Our measurements imply that the depth-averaged parameters would require the most adjustment near stagnation points.

Our observation that motions at the interface follow motions at the free surface raises questions and opens opportunity for further study. Is there a characteristic timescale by which the interface

lags the free surface? If so, does it vary with Reynolds number and/or layer thickness? How does it compare to the characteristic time for viscous coupling between the acid and oil? Since the free surface and interface are coupled primarily by viscosity, the viscous diffusion time $L^2/\bar{\nu}$ likely plays a key role. Future studies could address these and similar questions.

Finally, and more broadly, studying the interactions of coherent structures at the free surface and interface might reveal interesting physics. The methods described above are not limited to tracking vortex centroids found via the Okubo-Weiss parameter; many methods for locating LCS and/or ECS could be applied at both the free surface and the interface. Measuring coherent structures at both surfaces simultaneously might lead to a physics of interaction, and might be a useful, inexpensive step toward broader application of LCS and ECS in 3D flows.

ACKNOWLEDGMENT

We thank Balachandra Suri for sharing his code for computing the vertical velocity profiles and depth-averaged parameters.

[1] P. B. Rhines, Geostrophic turbulence, Annu. Rev. Fluid Mech. **11**, 401 (1979).
[2] R. H. Kraichnan, Inertial ranges in two-dimensional turbulence, Phys. Fluids **10**, 1417 (1967).
[3] C. E. Leith, Diffusion approximation for two-dimensional turbulence, Phys. Fluids **11**, 671 (1968).
[4] G. K. Batchelor, Computation of the energy spectrum in homogeneous two-dimensional turbulence, Phys. Fluids **12**, 233 (1969).
[5] M. R. Allshouse and T. Peacock, Lagrangian based methods for coherent structure detection, Chaos **25**, 097617 (2015).
[6] G. Haller, Langrangian coherent structures, Annu. Rev. Fluid Mech. **47**, 137 (2015).
[7] S. Balasuriya, N. T. Ouellette, and I. I. Rypina, Generalized lagrangian coherent structures, Physica D **372**, 31 (2018).
[8] D. Lucas and R. R. Kerswell, Spatiotemporal dynamics in two-dimensional Kolmogorov flow over large domains, J. Fluid Mech. **750**, 518 (2014).
[9] B. Suri, J. Tithof, R. O. Grigoriev, and M. F. Schatz, Forecasting Fluid Flows Using the Geometry of Turbulence, Phys. Rev. Lett. **118**, 114501 (2017).
[10] M. K. Rivera, W. B. Daniel, S. Y. Chen, and R. E. Ecke, Energy and Enstrophy Transfer in Decaying Two-Dimensional Turbulence, Phys. Rev. Lett. **90**, 104502 (2003).
[11] G. L. Eyink and H. Aluie, Localness of energy cascade in hydrodynamic turbulence. I. Smooth coarse graining, Phys. Fluids **21**, 115107 (2009).
[12] H. Aluie and G. L. Eyink, Localness of energy cascade in hydrodynamic turbulence. II. Sharp spectral filter, Phys. Fluids **21**, 115108 (2009).
[13] D. H. Kelley, M. R. Allshouse, and N. T. Ouellette, Lagrangian coherent structures separate dynamically distinct regions in fluid flows, Phys. Rev. E **88**, 013017 (2013).
[14] S. Gowen and T. H. Solomon, Experimental studies of coherent structures in an advection-reaction-diffusion system, Chaos **25**, 087403 (2015).
[15] T. D. Nevins and D. H. Kelley, Optimal Stretching in Advection-Reaction-Diffusion Systems, Phys. Rev. Lett. **117**, 164502 (2016).
[16] T. D. Nevins and D. H. Kelley, Front tracking for quantifying advection-reaction-diffusion, Chaos **27**, 043105 (2017).
[17] T. Chevalier, D. Salin, and L. Talon, Frozen fronts selection in flow against self-sustained chemical waves, Phys. Rev. Fluids **2**, 100 (2017).
[18] T. D. Nevins and D. H. Kelley, Front tracking velocimetry in advection-reaction-diffusion systems, Chaos **28**, 043122 (2018).

[19] E. Beauvier, S. Bodea, and A. Pocheau, Front propagation in a regular vortex lattice: Dependence on the vortex structure, Phys. Rev. E **96**, 053109 (2017).
[20] H. J. H. Clercx and G. J. F. van Heijst, Two-dimensional navier–stokes turbulence in bounded domains, Appl. Mech. Rev. **62**, 020802 (2009).
[21] N. F. Bondarenko, M. Z. Gak, and F. V. Dolzhanskii, Laboratory and theoretical models of plane periodic flow, Akademiia Nauk SSSR, Izvestiia, Fizika Atmosfery i Okeana **15**, 1017 (1979).
[22] A. Thess, Instabilities in two-dimensional spatially periodic flows. Part I: Kolmogorov flow, Phys. Fluids A **4**, 1385 (1992).
[23] A. Thess, Instabilities in two-dimensional spatially periodic flows. Part II: Square eddy lattice, Phys. Fluids A **4**, 1396 (1992).
[24] G. A. Voth, G. Haller, and J. P. Gollub, Experimental Measurements of Stretching Fields in Fluid Mixing, Phys. Rev. Lett. **88**, 254501 (2002).
[25] T. H. Solomon and I. Mezič, Uniform resonant chaotic mixing in fluid flows, Nature **425**, 376 (2003).
[26] D. H. Kelley and N. T. Ouellette, Onset of three-dimensionality in electromagnetic thin-layer flows, Phys. Fluids **23**, 045103 (2011).
[27] R. A. D. Akkermans, A. R. Cieslik, L. P. J. Kamp, R. R. Trieling, H. J. H. Clercx, and G. J. F. van Heijst, The three-dimensional structure of an electromagnetically generated dipolar vortex in a shallow fluid layer, Phys. Fluids **20**, 116601 (2008).
[28] R. A. D. Akkermans, L. P. J. Kamp, H. J. H. Clercx, and G. J. F. van Heijst, Intrinsic three-dimensionality in electromagnetically driven shallow flows, Europhys. Lett. **83**, 24001 (2008).
[29] J. Paret, D. Marteau, O. Paireau, and P. Tabeling, Are flows electromagnetically forced in thin stratified layers two dimensional? Phys. Fluids **9**, 3102 (1997).
[30] R. A. D. Akkermans, L. P. J. Kamp, H. J. H. Clercx, and G. J. F. van Heijst, Three-dimensional flow in electromagnetically driven shallow two-layer fluids, Phys. Rev. E **82**, 026314 (2010).
[31] B. Jüttner, D. Marteau, P. Tabeling, and A. Thess, Numerical simulations of experiments on quasi-two-dimensional turbulence, Phys. Rev. E **55**, 5479 (1997).
[32] M. P. Satijn, A. W. Cense, R. Verzicco, H. J. H. Clercx, and G. J. F. van Heijst, Three-dimensional structure and decay properties of vortices in shallow fluid layers, Phys. Fluids **13**, 1932 (2001).
[33] J. Tithof, B. C. Martell, and D. H. Kelley, Three-dimensionality of one- and two-layer electromagnetically driven thin-layer flows, Phys. Rev. Fluids **3**, 064602 (2018).
[34] B. Suri, J. Tithof, R. Mitchell Jr., R. O. Grigoriev, and M. F. Schatz, Velocity profile in a two-layer Kolmogorov-like flow, Phys. Fluids **26**, 053601 (2014).
[35] N. T. Ouellette, H. Xu, and E. Bodenschatz, A quantitative study of three-dimensional Lagrangian particle tracking algorithms, Exp. Fluids **40**, 301 (2006).
[36] Jerry Westerweel and Fulvio Scarano, Universal outlier detection for PIV data, Exp. Fluids **39**, 1096 (2005).
[37] See Supplemental Material at http://link.aps.org/supplemental/10.1103/PhysRevFluids.4.043904 for movies showing the motion of tracked particles and vortex centers, at both the free surface and the interface, for steady and chaotic flow (Re = 62 and 370, respectively).
[38] A. Okubo, Horizontal dispersion of floatable particles in vicinity of velocity singularities such as convergences, Deep-Sea Res. **17**, 445 (1970).
[39] J. B. Weiss, The dynamics of enstrophy transfer in two-dimensional hydrodynamics, Physica D **48**, 273 (1991).
[40] G. Haller, An objective definition of a vortex, J. Fluid Mech. **525**, 1 (2005).
[41] J. Tithof, B. Suri, R. K. Pallantla, R. O. Grigoriev, and M. F. Schatz, Bifurcations in a quasi-two-dimensional Kolmogorov-like flow, J. Fluid Mech. **828**, 837 (2017).